



A novel methodology for design optimization of heat recovery steam generators with flow-induced vibration analysis

Han Deng^{a,*}, Geir Skaugen^a, Erling Næss^b, Mingjie Zhang^b, Ole A. Øiseth^b

^a SINTEF Energy Research, P.O. Box 4761 Torgarden, NO-7465, Trondheim, Norway

^b Norwegian University of Science and Technology, NO-7491, Trondheim, Norway

ARTICLE INFO

Article history:

Received 12 November 2020

Received in revised form

7 February 2021

Accepted 5 March 2021

Available online 15 March 2021

Keywords:

Heat recovery steam generator (HRSG)

Design optimization

Flow-induced vibration

Vibration analysis

Finned tube bundles

ABSTRACT

Design of compact, lightweight, and robust heat recovery steam generators (HRSGs) is important for the implementation of offshore bottoming cycles. In this work, a novel methodology integrating flow-induced vibration analysis is proposed for the design optimization of HRSG. The vibration analysis considers four main flow-induced vibration mechanisms, namely turbulent buffeting, vortex shedding, fluidelastic instability, and acoustic resonance. The corresponding sub-models are selected from literature for estimating vibrations of finned tube bundles. The design criteria for vibration are included in the optimization problem as constraints, which affect the decision of the solver simultaneously. The methodology is demonstrated by three cases, in which not only geometric parameters but also operating parameters are set as design variables. With activating vibration constraints, the solver finds appropriate geometric and operating parameters to meet the design requirements. The comparison between the optimizations with and without the vibration constraints shows a trade-off between compactness, lightweight, efficient heat transfer, and the possibility of flow-induced vibration problems. This indicates the importance of consideration of vibration problems when designing such HRSGs.

© 2021 The Author(s). Published by Elsevier Ltd. This is an open access article under the CC BY-NC-ND license (<http://creativecommons.org/licenses/by-nc-nd/4.0/>).

1. Introduction

Offshore oil and gas production is an energy-intensive process, and the Norwegian oil and gas offshore section has contributed about 20–30% to the total Norwegian CO₂-emissions in the last decade [1]. The emissions per produced oil equivalent were reduced by approximately 19% from 1990 to 2005 [2], which is the result of a combination of improved energy efficiency mainly caused by reduced natural-gas flaring and installation of waste heat recovery units [3]. A bottoming cycle, added to the gas turbines powering offshore oil and gas installations, can recover waste heat from the exhaust gas and thus increase the energy efficiency of plants. However, the bottoming cycles have not been widely implemented on offshore platforms, due to the restrictions on weight, footprint, and volume [4].

Heat recovery steam generator (HRSG) is one of the key components in a steam bottoming cycle and contributes the majority of the weight of bottoming cycles. A simple HRSG is composed of an economizer, an evaporator, and a superheater. These heat

exchanger units are bare and finned tubes integrated with collector headers and interconnecting piping systems [5]. The optimization of HRSG concerning compactness, lightweight, and robustness is of significance to increase the utilization of bottoming cycles on offshore platforms. For this purpose, the optimization model usually requires a detailed description of heat exchanger units and HRSG structures, and enables the geometric parameters as variables.

Franco and Giannini [6] proposed a methodology with a two-level optimization of HRSG. The first level enables to obtain operating parameters with the objective of minimizing thermal exergy losses, and the second level involves a detailed design of heat transfer sections with geometric variables and the objective of HRSG compactness defined as effective heat transfer surface to volume. They applied the optimization process for an existing combined cycle plant with a double-pressure HRSG, and achieved a reduction of 25% in exergy losses with an increase of 8% in total core volume and 16.7% increase in compactness.

Manassaldi et al. [7] investigated the optimal design of HRSG applying different objective functions: net power, ratio of net power and material weight, and net heat transfer. Operating parameters and geometric parameters are set as continuous and integer

* Corresponding author.

E-mail address: han.deng@sintef.no (H. Deng).

Nomenclature		y	Tube deflection, [m]
c	Speed of sound, [m s ⁻¹]	<i>Greek Symbols</i>	
d	Diameter, [m]	δ	Logarithmic decrement, [–]
d_h	Hydraulic diameter, [m]	ρ	Density, [kg m ⁻³]
E	Young's modulus, [Pa]	σ	Volume fraction of the bundle occupied by tubes and fins, [–]
F	Force, [N]	<i>Subscripts</i>	
f_a	Acoustic resonance frequency, [Hz]	eff	Effective
f_n	Natural frequency, [Hz]	f	Fin/Finned tubes
f_{vs}	Vortex shedding frequency, [Hz]	fl	Fluid
g	Fin tip clearance, [m]	i	Inside tube
h	Fin height, [m]	o	Outside tube
I	Second moment of inertia, [m ⁴]	t	Tube
j	Mode number, [–]	vs	Vortex shedding
L	Length of tube span, [m]	<i>Abbreviation</i>	
m	Mass per unit length, [kg m ⁻¹]	HRSG	Heat recovery steam generator
p	Pitch, [m]	cstr	constraints
S	Power spectral density	opt	optimization
s	Fin space, [m]	vib	vibration
Sr	Strouhal number, [–]		
t	Fin thickness, [m]		
U	Flow velocity, [m s ⁻¹]		

variables, respectively. They concluded that the optimal configuration and operating conditions highly depend on the objective function used, and global optimal solutions cannot be guaranteed.

Rezaie et al. [8] developed an optimization model to minimize the cost of HRSG using a genetic algorithm, in which a comprehensive thermal design is provided. By appropriately selecting finned tube specifications and arrangements, the overall heat transfer rate was increased and the heat transfer surface area was decreased when applying the method to an existing HRSG with the same operating conditions. A reduction of 24.3% in capital cost and 23.1% in total weight was reported for the optimized HRSG compared to the existing one.

Mehrgoo and Amidpour [9,10] proposed a model to simultaneously optimize the operating and geometric design parameters of the HRSG by using the constructal theory. The optimization for a dual pressure HRSG was conducted for minimizing the exergy destruction rate with a size constraint for the volume of the heat transfer sections [9]. They concluded that there exists an optimal value for the HRSG volume and further increasing the heat transfer area (bigger volume) has a marginal effect on the heat recovery and exergy generation. With the same method, they performed studies for single, dual and triple pressure HRSGs with several objective functions subject to the volume constraint [10]. The triple pressure HRSG was found to have the largest heat recovery in the three configurations.

Skaugen et al. [11] proposed a heat exchanger model and performed optimization for waste heat recovery unit with detailed consideration on the weight of heat exchanger core and structural elements, e.g. support and frame beams, inlet and outlet ducts. It was found that the optimized geometries are similar when using minimum core weight and total weight as objective functions. Besides, they pointed out that to utilize a lighter heat exchanger, vibration analysis and mechanical design rules need to be considered.

The optimization works from literature focus mostly on thermal and economic performances of HRSGs, while structural performance such as vibration problems is less addressed. Industrial operations of steam generators and heat exchangers have revealed flow-induced vibration may seriously impact the structural fatigue

life and/or safety. Many real-life cases in which flow-induced vibrations result in serious damages were introduced by Paidoussis [12]. The expensive consequences of these cases significantly advanced the necessity to achieve a structural design robust to flow-induced vibration. To the authors' knowledge, there is no optimization model for HRSG that includes design criteria for flow-induced vibrations simultaneously with other performance requirements. Vibration analysis is mostly performed after the thermal design and will not influence the design directly, such as the works [13,14]. In order to investigate how vibration criteria affect the design, we consider the vibration analysis during the optimization procedure formulated as additional constraints.

The main contributions of this work include:

1. We present a novel methodology for the design optimization of HRSG. The method integrates the heat exchanger model and the flow-induced vibration models for finned tube bundles. Several design criteria for vibrations are implemented as inequality constraints to the optimization solver. In this way, the optimization with the aim of minimizing HRSG weight can ensure an optimal design satisfying all the thermal, hydraulic, and structural design requirements. To our knowledge, this is the first time that vibration analysis and design criteria is used to directly affect decision variables for the optimization of HRSG geometry.
2. Optimizations with and without vibration constraints are performed for three cases for demonstrating the methodology and how vibration constraints alter the HRSG geometries and operating conditions.
3. The optimization model uses both geometric and operating parameters as free design variables.
4. The model deals with the optimization of HRSGs with a single heat exchanger unit, as well as multiple units of independent geometries in a bottoming cycle.

The rest of this article is organized as follows. Section 2 describes the methodology. The case definitions, optimization results, and discussion are given in Section 3. The conclusions are made in Section 4.

2. Methodology

This section presents the optimization methodology. A brief description of the problem is given in Section 2.1. Section 2.2 describes the definitions of the HRSG geometries and weight components related to the variables and objective function of the optimization model. Thermal-hydraulic models of HRSG are described in Section 2.3. The flow-induced vibration models related to constraints of the optimization model are presented in Section 2.4. The optimization procedures are provided in Section 2.5.

2.1. Problem description

The present work considers a single or multi-core once-through HRSG recovering the exhaust heat from gas turbines. The problem is to optimize the design of HRSG for a minimum weight, which satisfies operating requirements and design criteria to limit flow-induced tube vibration.

2.2. Geometries and weight components of HRSG

The heat exchanger core is a finned tube bundle type, as illustrated in Fig. 1. The exhaust gas flows vertically outside the finned tubes, while water/steam flows horizontally inside the tubes in cross-counter flow to the exhaust gas. As an example, the tube bundle has 10 tube passes and 2 tubes per pass, which gives a total of 20 tube rows along the exhaust gas flow. The bundle width is defined as the steam-flow length in a tube row excluding bends, and the bundle depth is the exhaust-flow length along all the tube rows. The bundle height is the length of stacked tubes per row, whose direction is transversal to the exhaust gas flow. Fig. 1b depicts the geometries of tubes and fins on the cross section perpendicular to the steam-flow direction. Staggered tube arrangement with 30° layout are defined for the tube bundle. Plain circular fins are used here.

In addition to the tube bundle, the structural elements are the main contributors to the total weight of HRSG, as shown in Fig. 2. The HRSG structure consists of three parts as depicted in Fig. 2a, an inlet transition duct, a core ‘envelope’ around the tube bundle, and an exit transition duct. The casing of these parts is made up of an inner lining, an insulation layer, and an outer duct plate. Each part is supported by frame beams (in grey) and support beams (in green)

as illustrated in Fig. 2b. Additionally, the weight of the core envelope includes the weight of support plates and beams (in red) for the tube bundle.

With specifying the inspection room in the three dimensions, namely the distances between the edges of the bundle to the inner frame wall, the dimensions of the core envelope can be obtained. The inlet and exit transition ducts are characterized by cross-sectional area and transition angle. In the example given in Fig. 2a, the cross section of the inlet and exit duct is fixed at $1\text{ m} \times 1\text{ m}$, and the transition angle is defined as 25° and 50° , respectively. The dimensions of the inlet and exit ducts can be calculated when knowing the dimensions of the core envelope. This implies that the duct weight is directly dependent on the core size and will in turn affect the layout of the tube bundle when optimizing for a minimum total weight of HRSG. An alternative to the transition angle would be to specify the duct flow length. The input parameters for calculating dimensions and weight of HRSG are provided in the supplemental file. The total weight of HRSG defined in the current work is the sum of the weight of the tube bundle and the weight of frames and ducts. Details regarding the methods of weight calculation can be found in Ref. [11].

2.3. Thermal-hydraulic model of the tube bundle

The thermal-hydraulic simulation of the tube bundle employs an in-house heat exchanger modeling tool [15]. The model uses the geometry of the tube bundle and inlet conditions of fluids as input, and calculates heat transfer and pressure loss. The tube bundle is discretized along the width and depth. The enthalpy and pressure of the exhaust gas outlet are guessed as the initial value for iteration. The heat transfer and pressure drop for the first element of steam flow are then calculated with the known inlet conditions of steam and outlet conditions of exhaust gas, and the steam outlet and exhaust gas inlet conditions at this element can be obtained and used as input to the next element. After the calculation finishes for the last element, the calculated inlet conditions of exhaust gas are compared with the specified values. The residuals are used to update outlet conditions of exhaust gas for the next iteration. The iteration finishes when the residuals are smaller than the prescribed tolerance. The non-linear set of equations are solved using the DNSQE-routine from SLATEC [16].

The heat exchanger model requires heat transfer and pressure

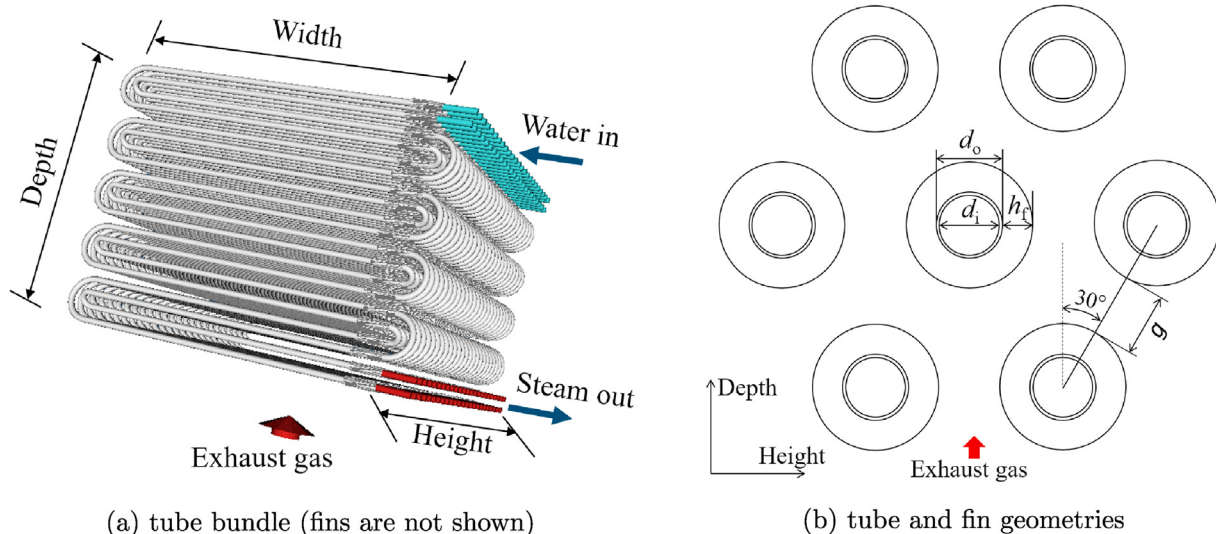


Fig. 1. Main geometries of a finned tube bundle.

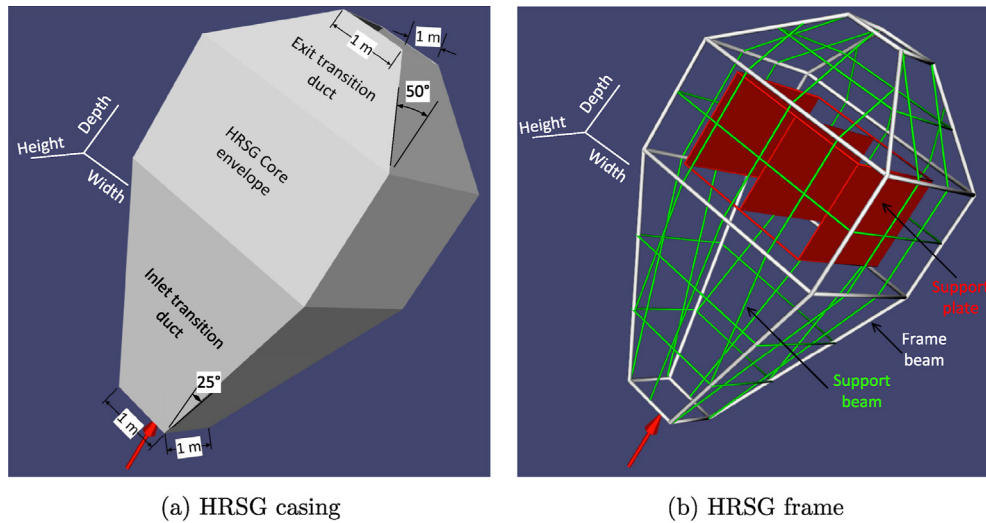


Fig. 2. Main structural components of HRSG: casing and frame.

drop correlations suitable for specific types of heat exchangers. The ESCOA correlation [17] is used for calculating pressure drop and heat transfer coefficient of exhaust gas flowing outside the finned tube bundle. The heat transfer coefficient of water/steam flowing inside tubes is evaluated from the Gnielinski correlation [18] for single-phase flow, and Bennet and Chen [19] for evaporation. The water/steam pressure drop is calculated from correlations by Selander [20] for single-phase flow and Friedel [21] for two-phase flow.

To test and validate the heat exchanger model, the simulation results are compared with the data obtained from an once-through HRSG of pilot plant size reported by Dumont and Heyen [22]. The heat exchanger model is run as a ‘simulator’ with the given geometry and inlet conditions. The calculated outlet temperatures of the exhaust gas and water are compared with the reference data from the HRSG. The results show good agreement with an absolute difference in the temperature smaller than 5 °C and a relative difference in the heat capacity of 0.4%. The data of the HRSG and comparison with simulation results are provided in the supplemental file.

2.4. Vibration analysis

The vibration excitation mechanisms considered for tube bundles in cross-flow configuration include turbulent buffeting, vortex shedding, fluidelastic instability, and acoustic resonance [23]. Turbulent buffeting is a type of forced vibration with moderate amplitude excited by the random turbulence [24,25]. Vortex shedding excitation is a periodic excitation with one dominate frequency. Intensive vibrations may be excited as the dominant frequency of periodic vortex shedding approaches one of the natural frequencies of the tube [26]. Fluidelastic instability is a mechanism that produces destructive self-excited vibration once a critical flow velocity is exceeded [27,28]. Acoustic resonance may be generated by the coincidence between one of the acoustic modes of the duct and the dominant frequency of vortex shedding or turbulent buffeting [29,30]. Detailed discussions of these flow-induced vibration mechanisms are found in review papers [31–33] and books [34,35].

2.4.1. Finned tube parameters

For each vibration mechanism, we selected acceptance criteria

from literature. These are related to several important parameters describing tube and tube bundle characteristics, such as tube natural frequency and system damping. The natural frequency of a single span tube can be calculated from Ref. [36],

$$f_{n,j} = \frac{\lambda_j^2}{2\pi L^2} \sqrt{\frac{EI}{m_{eff}}} \sqrt{1 + \frac{F_{ax}}{F_{cr}}} \quad (1)$$

where λ^2 is a dimensionless parameter depending on the end fixation of the tube span and mode number j , L is the length of the span between supports, E is the material Young’s modulus, I is the second moment of inertia of the tube, F_{ax} and F_{cr} are the axial force and Euler’s buckling force acting on the tube. The last term related to the forces on the tube is not considered and neglected in the present work. The effective mass per unit length of the tube with the fins characterized by fin pitch p_f , fin thickness t_f , fin height h_f , is obtained as,

$$m_{eff} = \frac{\pi}{4} \rho_t (d_o^4 - d_i^4) + \frac{\pi}{4} (\rho_{fl,i} d_i^2 + k \rho_{fl,o} d_o^2) + \frac{\pi t_f \rho_f}{4 p_f} [(d_o + 2h_f)^2 - d_o^2] \quad (2)$$

where k is an added mass factor. With gas flowing external to the tubes, the added mass term is small and negligible.

The attached fins will increase the dynamic stiffness of the tube. Using the moment of inertia of the plain tube will tend to underestimate the tube natural frequency. Thus, the moment of inertia is corrected to take into account the effect of the fins with using the model from Bolleter and Blevins [37],

$$I_{eff} = p_f \left(\frac{s_f}{I} + \frac{t_f}{I_f} \right)^{-1} \quad (3)$$

with

$$I = \frac{\pi}{64} (d_o^4 - d_i^4), \quad I_f = \frac{\pi}{64} [(d_o + t_f/2)^4 - d_i^4] \quad (4)$$

where the space between two fins $s_f = p_f - t_f$.

The damping of the vibration is due to structural damping, support damping, and viscous damping with the fluid surrounding

the tube. Viscous damping with low-pressure gas on the outside of the tube is insignificant and neglected here. The system damping including the structural damping and support, expressed in a logarithmic decrement δ , is calculated with the model by Gelbe and Ziada [38].

2.4.2. Turbulent buffeting

The acceptance criterion for turbulent buffeting vibration is set in terms of a maximum allowable tube vibration, which should be within 2% of the tube outer diameter. For a plain or finned tube, the response to turbulent buffeting considering only the first tube natural frequency (fundamental mode) can be estimated from Ref. [33],

$$y_{rms} = \frac{1}{16\pi} \sqrt{\frac{2S\varphi_1^2 a_1 d_h^3 \rho_{fl,o}^2 U_{max}^3}{L f_n^3 m_{eff}^2 \delta}} \quad (5)$$

where y_{rms} is the root mean square of tube deflection, d_h is the hydraulic diameter of plain or finned tube, and U_{max} is the external fluid velocity in the minimum free-flow passage. The natural frequency f_n represents the one at mode 1 if not specified hereafter. The parameter S is the turbulent power spectral density, φ_1 is the normalized mode shape for mode 1, and a_1 is the first mode dimensionless coefficient for the modal joint acceptance. The expressions and values of these parameters can be referred to Pettigrew and Taylor [33]. The hydraulic diameter for the finned tubes is obtained with the model by Halle et al. [39],

$$d_{h,f} = \frac{s_f d_o + t_f (d_o + 2h_f)}{p_f} \quad (6)$$

2.4.3. Vortex shedding

The criterion for the vortex shedding is to either avoid the lock-in of the vortex shedding frequency to tube natural frequency or to limit the tube vibration amplitude within 2% of tube outer diameter when the lock-in occurs. The lock-in conditions can be estimated as,

$$0.8 < f_{vs}/f_n < 1.2 \quad (7)$$

The frequency of vortex shedding is determined by Strouhal number (Sr),

$$f_{vs} = \frac{Sr \cdot U_{max}}{d_h} \quad (8)$$

The Strouhal number is calculated by the empirical model by Pettigrew and Taylor [33], which was developed from experimental data by Weaver et al. [40].

The tube response due to the vortex shedding can be related to the lift force F_L imposed on the tubes by the vortices with the model from Ref. [41],

$$y_{vs,rms} = \frac{F_L}{\sqrt{2\pi^2 f_n^2 m_{eff} \delta}} \quad (9)$$

The lift force employs the model by Pettigrew and Taylor [33].

2.4.4. Fluidelastic instability

The acceptance criterion for fluidelastic instability is that the maximum external flow velocity U_{max} is lower than the critical velocity. A safety factor of 0.8 is used for conservatism. The critical velocity is derived from the empirically developed model by Connors [27],

$$\frac{U_{crit}}{f_n d_h} = K \sqrt{\frac{m_{eff} \delta}{\rho_{fl,o} d_h^2}} \quad (10)$$

where K is the fluidelastic instability constant, recommended as 3.0 for finned tube bundles by Pettigrew and Taylor [32].

2.4.5. Acoustic resonance

The lock-in of acoustic resonance frequency to the shedding frequency is determined from Ref. [33],

$$0.8 < f_{a,j}/f_{vs} < 1.35 \quad (11)$$

The ratio $f_{a,j}/f_{vs}$ outside the lock-in condition is set as the acceptance criterion. Pettigrew and Taylor [33] recommended calculating the acoustic resonance frequencies for the first few acoustic modes (i.e., the first five modes should suffice).

The acoustic resonance frequency is defined as,

$$f_{a,j} = \frac{c_{eff}}{2} \frac{j}{H} \quad (12)$$

where c_{eff} is the effective speed of sound in the tube bundle, and H is the distance between the duct walls normal to the external flow direction and tube axis. The effective speed of sound is lower than the speed of sound of gas c_0 due to the existence of tubes, and can be corrected as [42],

$$c_{eff} = \frac{c_0}{\sqrt{1 + \sigma}} \quad (13)$$

where σ is defined as the volume fraction of the bundle occupied by tubes and fins.

2.5. Optimization with vibration constraints

The optimization model employs the gradient-based constrained optimization solver NLPQL [43]. The objective is to minimize the total weight of HRSG, subjected to a set of equality and inequality constraints. The vibration acceptance criteria are implemented as inequality constraints which have to be positive for the problem to be solved. The equality constraints, such as the required duty, need to be equal to their specified values. The free variables for the optimization problem can be both geometric and operating parameters depending on the case. All free variables are restricted by an upper and lower bound.

For a given set of input variables, the heat duty and pressure loss of the heat exchanger core are solved according to the method described in Section 2.3. The partial derivatives of the objective and constraint functions are estimated by the central difference method. The gradient information is used by the NLPQL solver to provide new estimates for the free variables for the next iteration. The problem is solved when the minimum value of the objective function is found and all the constraints are satisfied.

For each iteration, the four types of vibration are calculated row by row following the exhaust gas flow. Depending on the number of support plates, the tubes are divided into end spans and middle spans, of which natural frequency will be different due to end fixation and length. The number of support plates here excludes the two plates at the sides. Fig. 3 shows examples with tubes of one and two end spans, and multiple spans. The ends of the tube span are fixed to two side plates (e.g. Fig. 3a), while tube spans are hinged to the middle plates in Figs. 3b and 3c. At present, the length of end spans and middle spans are evenly distributed based on the number of support plates. The tube deflections due to turbulent

buffeting and vortex shedding, and the critical velocity related to fluidelastic instability will be calculated for both end span and middle spans. The maximum values at the end spans and middle spans among all the tube rows will be identified and used in the evaluation of the constraint functions. For acoustic resonance, we currently consider the first two modes and restrict the ratio of the acoustic resonance frequency for the second mode to the vortex shedding frequency higher than the upper boundary (1.35) of the lock-in condition (Eq. (11)). This limits the number of constraints and also ensures that the frequencies at higher modes ($j \geq 3$) satisfy the criterion. The constraint functions for the four vibration mechanisms are summarized in Table 1.

3. Results and discussion

For demonstrating the optimization model and the impact of vibration constraints, three cases are considered.

- (I) a single-core HRSG without support plates (Fig. 3a), with specifying heat duty and optimizing only geometric variables;
- (II) a single-core HRSG with one center support plate (Fig. 3b), with specifying heat duty and optimizing only geometric variables;
- (III) a three-core HRSG with multiple support plates (Fig. 3c) in a bottoming cycle, with specifying net power output from the cycle and optimizing geometric and operating variables simultaneously.

Case (I) and case (II) are a scaled-down version of an existing heat recovery unit and exhaust gas conditions, and case (III) represents a full hypothetical offshore bottoming cycle. For each case, the results from optimizations with active and inactive vibration constraints will be compared.

3.1. Single-core HRSG without support plates

The operating conditions of the exhaust gas and steam are listed in Table 2, whereas the settings of variables and constraints are summarized in Table 3. An important inequality constraint is the maximum allowable pressure drop of the exhaust gas, which is necessary to keep the acceptable back pressure of gas turbines. The optimization with active vibration constraints includes the additional constraints listed in Table 1. Except for the parameters given in Table 3, the tube wall thickness is determined from the tube inner diameter, design pressure, and allowable stress of the tube material.

The results from the vibration analysis for case (I) are shown in

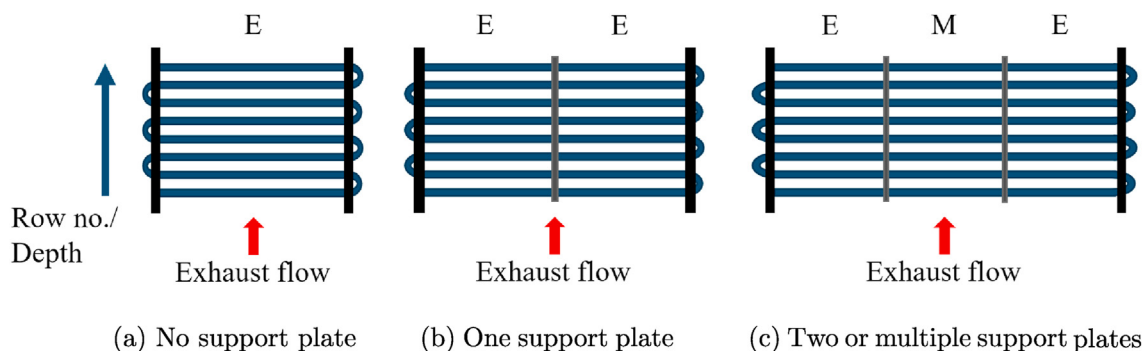


Fig. 3. Tube spans with the different number of support plates (E: end span, M: middle span).

Table 1
Inequality constraints for vibration analysis in the optimization model.

Vibration mechanism	Constraint functions
Turbulent buffeting	$0.02 - y_{rms}/d_o \geq 0$
Vortex shedding	$0.02 - y_{vs,rms}/d_o \geq 0$, if $0.8 < f_{vs}/f_n < 1.2$
fluidelastic instability	$0.8 - U_{max}/U_{crit} \geq 0$
Acoustic resonance	$(f_{a,1}/f_{vs} - 1.35)(f_{a,1}/f_{vs} - 0.8) \geq 0$ $f_{a,2}/f_{vs} - 1.35 \geq 0$

Table 2
Operating conditions for the single-core HRSG in cases (I) and (II).

	Exhaust gas	Steam
Flow rate [kg s^{-1}]	24	2.75
Inlet temperature [$^{\circ}\text{C}$]	538	38.25
Inlet pressure [bar]	1.065	25

Table 3
Setting of variables, constraints, and fixed parameters for the optimization in cases (I) and (II).

Category	Parameter	Value/Range
Variables	Bundle width [m]	[2,3]
	Tube inner diameter [mm]	[12,35]
	Fin tip clearance [mm]	[2, 70]
	Fin pitch [mm]	[2,15]
	Fin height [mm]	[4,15]
	No. of tubes per row [-]	[12, 50]
Equality constraint	Heat duty [MW]	8.5
Inequality constraints	Max gas pressure drop [kPa]	1
	Max steam pressure drop [kPa]	100
	Max gas velocity [m s^{-1}]	35
	No. of passes [-]	11
Fixed parameters	No. of rows per pass [-]	3
	Fin thickness [mm]	0.8

Fig. 4, where the optimizations without the vibration constraints (blue line with circles) and with the vibration constraints (green line with squares) are compared. Four parameters indicating the four vibration mechanisms are plotted for each tube row in the direction of the exhaust gas flow, and row no. 1 is the one closest to the exhaust inlet. The red areas in the four plots represent the region where the constraint functions corresponding to the four vibration mechanisms in Table 1 are not satisfied. It can be seen that in the optimization without the vibration constraints, the design does not meet the vibration criteria for fluidelastic instability and the acoustic resonance, given that the points fall in the red region in Figs. 4c and 4d. With the vibration constraints, the solver can find a feasible design to mitigate flow-induced vibrations and meet the

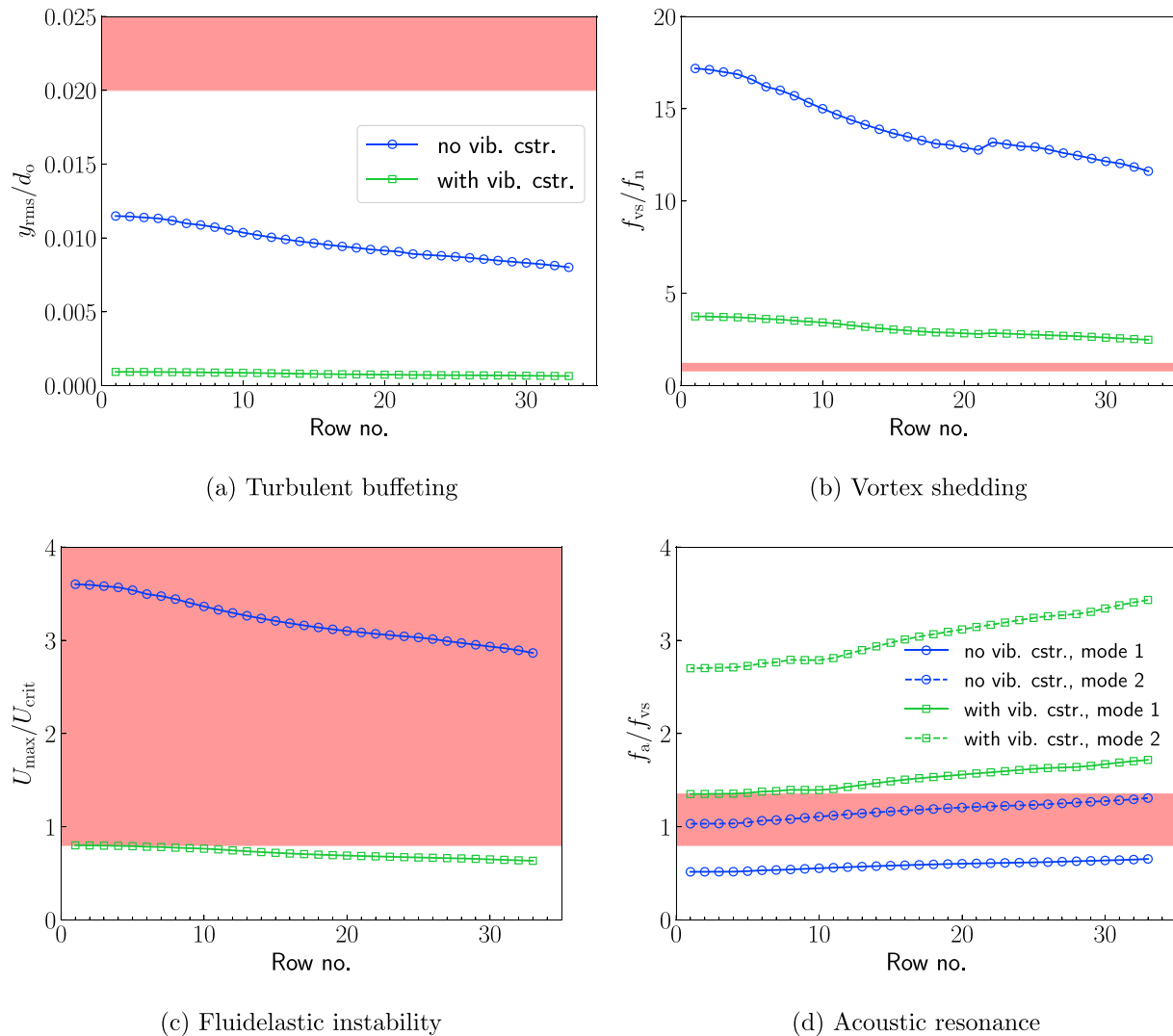


Fig. 4. Comparison of vibrations from the optimizations without (blue) and with (green) the vibration constraints for case (I). Red region represents where the criterion is not satisfied. Row no. 1 is the closest to the inlet of the exhaust gas. (For interpretation of the references to colour in this figure legend, the reader is referred to the Web version of this article.)

design criteria.

Fig. 4a shows that the tube deflection due to turbulent buffeting is decreased with the increase of the row number. The maximum deflection occurs at the first tube row for a given tube bundle, where the exhaust gas has the lowest density and thus the largest flow velocity. Meanwhile, the superheated steam inside the tube has the lowest density and gives a lowest mass for the first tube

Table 4
Variables of optimized HRSGs for case (I) and calculated geometric parameters.

	Opt. without vib. cstr.	Opt. with vib. cstr.
Bundle width [m]	2.13	2.05
Fin tip clearance [mm]	21.76	61.08
No. of tubes per row [-]	42	21
Tube inner diameter [mm]	12.00	26.08
Fin pitch [mm]	6.10	3.29
Fin height [mm]	5.63	14.56
Bundle height [m]	2.00	2.51
Bundle depth [m]	1.36	3.41
Heat transfer area [m ²]	492.5	1891.2
Core volume [m ³]	5.8	17.6

row. Without the vibration constraints, the tube deflection at the first row is 1.1% of the tube outer diameter, within the limit of 2%. With vibration constraints, the tube deflection significantly decreases in both the ratio to the tube outer diameter and the absolute value. This is the result of the re-arrangement of tube layout and finned tube geometries, as indicated by the optimized variables in Table 4.

The vortex shedding frequency, as given in Fig. 4b, is much higher than the tube natural frequency in the optimizations with and without the vibration constraints. This is consistent with the statement that normal flow velocities in gas heat exchangers are usually much higher than those required for vortex shedding resonance [33]. Including the vibration constraints, the vortex shedding frequency is reduced, which is mainly caused by a design giving a lower gas velocity and a larger hydraulic diameter (Eq. (8)). Currently, we only consider the lock-in condition for mode 1. Even when vortex shedding resonance occurs at higher modes, it is usually not a problem for this case as the gas density is too low to cause significant periodic forces [33] as well as tube vibration amplitude (Eq. (9)). The kink at tube row 22 (blue line) is due to a relatively large decrease of tube natural frequency, at which the

flow inside tube changes from two-phase into liquid phase and results in a sudden increase in density affecting the effective mass per unit length m_{eff} .

The large gas velocity from the optimization without the vibration constraints may lead to fluidelastic instability, as illustrated in Fig. 4c. With the vibration constraints, the ratio of the maximum local velocity to the critical velocity is reduced to below 0.8 for all the tube rows. It is a combined effect from the decreased gas velocity due to larger fin tip clearance and the increased critical

Table 5
Weight distribution of optimized HRSGs for case (I).

Weight [kg]	Opt. without vib. cstr.	Opt. with vib. cstr.
Tube	1507.1	2252.9
Fin	1033.4	5188.1
Core	2540.5	7441.0
Inlet transition duct	5413.3	7611.6
Core envelope	3925.8	9514.9
Exit transition duct	2369.5	3419.5
Frame and casing	11708.6	20546.0
Total	14249.1	27987.0

velocity due to higher natural frequency and effective mass per unit length (Eq. (10)). As shown by Eqs. (1) and (10), the optimized geometries with the vibration constraints given in Table 4, have a higher critical velocity for fluidelastic instability due to the shorter tube span and larger tube diameter (increased moment of inertia).

Fig. 4d displays the ratios of the acoustic resonance frequencies for the first and second modes to the vortex shedding frequency. The second mode frequency from optimization without the vibration constraints is close to the vortex shedding frequency, thus acoustic resonance may occur. Including the vibration constraints, the frequency ratios f_a/f_{vs} for the two modes are pushed above the upper limit of the lock-in condition. Only a small variation in the acoustic resonance frequency is observed, so the decrease of the vortex shedding frequency is the main reason for this.

The vibration analysis from the optimizations is consistent with the conclusion on the likelihood of the four vibration mechanisms by Pettigrew et al. [23]. For tube bundles with gas flow, the fluidelastic instability and acoustic resonance are the most important ones, while the occurrences of turbulent buffeting and vortex shedding are possible and unlikely, respectively.

As listed in Table 4, the fin tip clearance, tube inner diameter, and fin height are increased significantly after adding the vibration

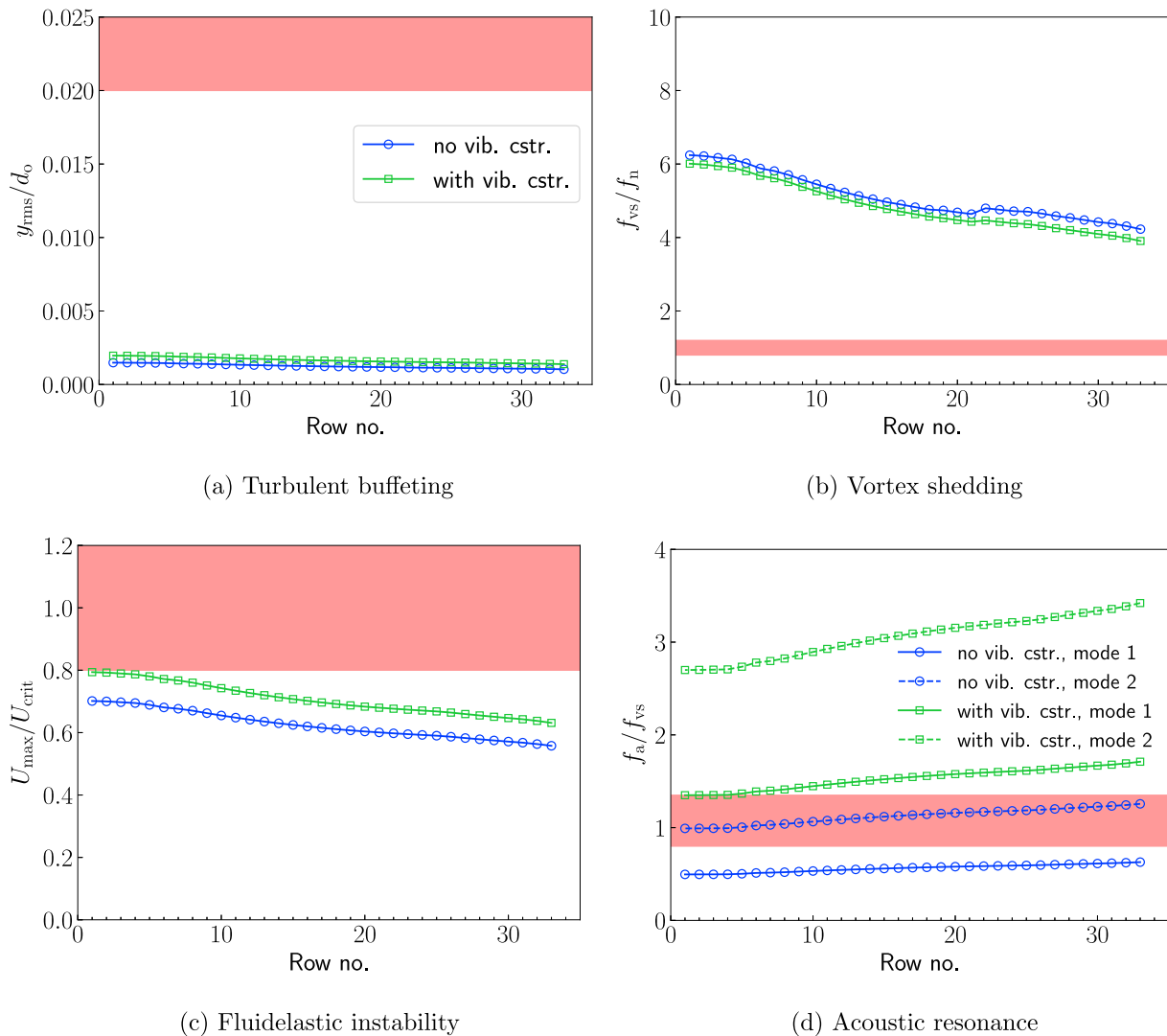
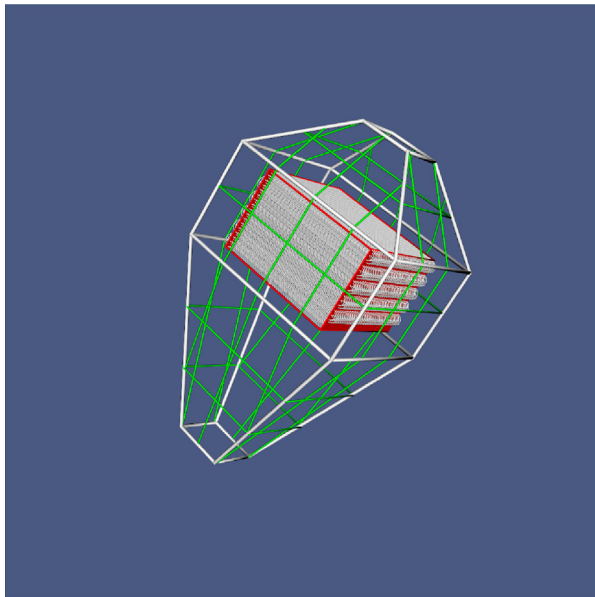
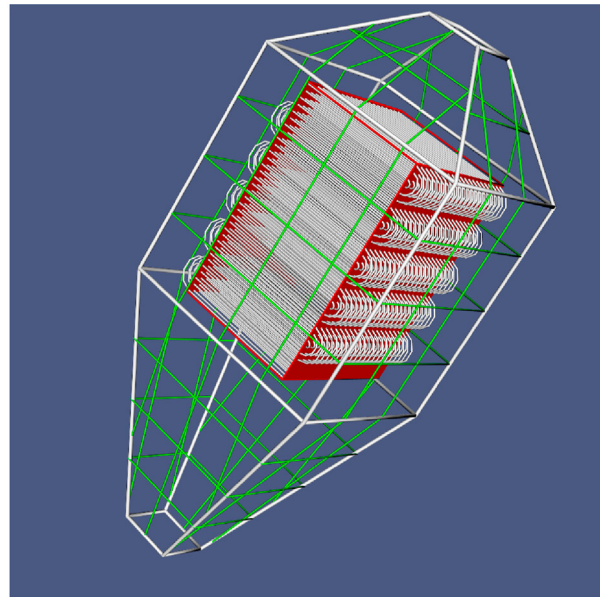


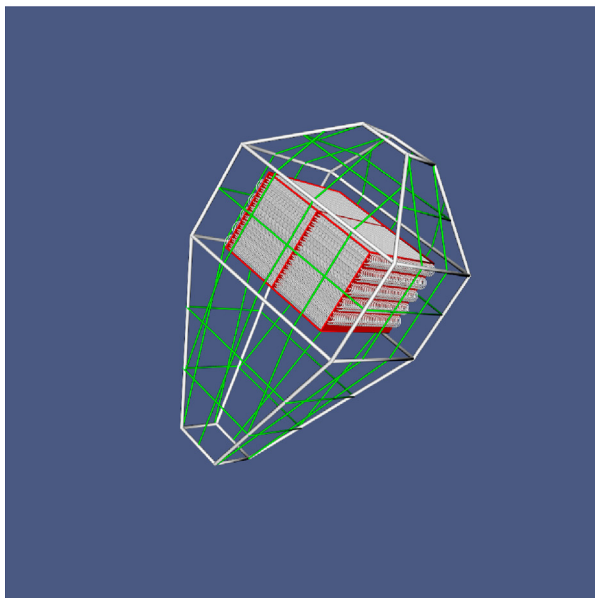
Fig. 5. Comparison of vibrations from the optimizations without (blue) and with (green) the vibration constraints for case (II). Red region represents the criterion is not satisfied. (For interpretation of the references to colour in this figure legend, the reader is referred to the Web version of this article.)



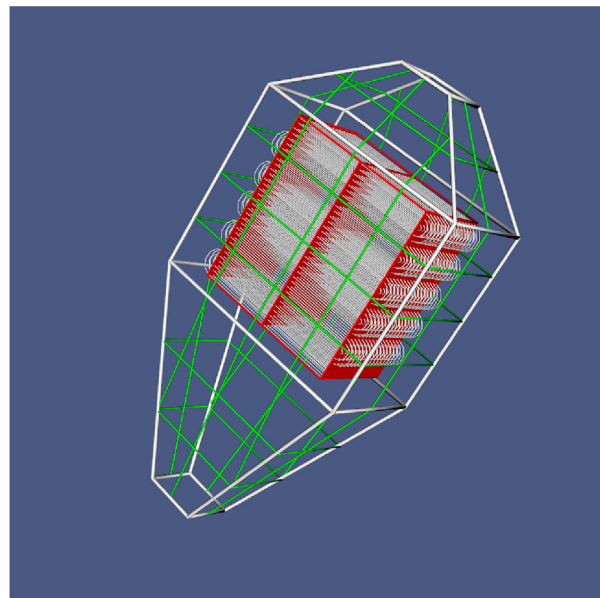
(a) No support plate, no vibration constraints



(b) No support plate, with vibration constraints



(c) One support plate, no vibration constraints



(d) One support plate, with vibration constraints

Fig. 6. Visualization of HRSGs optimized for cases (I) and (II).

Table 6
Variables of optimized HRSGs for case (II) and calculated geometric parameters.

	Opt. without vib. cstr.	Opt. with vib. cstr.
Bundle width [m]	2.13	2.48
Fin tip clearance [mm]	21.02	56.86
No. of tubes per row [-]	43	16
Tube inner diameter [mm]	12.00	13.59
Fin pitch [mm]	6.20	2.77
Fin height [mm]	5.45	10.82
Bundle height [m]	2.01	1.53
Bundle depth [m]	1.33	2.70
Heat transfer area [m ²]	486.7	968.0
Core volume [m ³]	5.7	10.3

Table 7
Weight distribution of optimized HRSGs for case (II).

Weight [kg]	Opt. without vib. cstr.	Opt. with vib. cstr.
Tube	1552.6	803.6
Fin	1004.2	2625.1
Core	2556.8	3428.7
Inlet transition duct	5446.7	5641.4
Core envelope	4065.5	6880.3
Exit transition duct	2386.1	2401.0
Frame and casing	11898.4	14922.6
Total	14455.2	18351.3

constraints, which results in a large increase of the bundle depth. Even though the number of tubes per row becomes less, the bundle (stacking) height is increased due to the increased fin tip clearance. This results in a lower gas velocity and thus a lower heat transfer rate. The heat transfer surface at the exhaust gas side is enlarged about four times to fulfill the required heat capacity, with the increase mainly from the fin area by denser (smaller fin pitch) and larger fins (larger fin height).

Table 5 gives the weight of the main components for the optimized HRSG design with and without the vibration constraints. The core weight is the sum of the weight of the tubes and fins, while the total weight is composed of core weight and weight of the structural elements described in Section 2.2. It can be seen that the minimum total weight is almost doubled in order to satisfy the vibration criteria. The increase of the total weight mainly comes from the weight of the core envelope and fins. The increase of the frame weight is due to the larger dimensions of the tube bundle. This suggests that for the current operating conditions, the use of an additional support plate is necessary. A graphic illustration of the HRSGs will be provided together with the following case in Fig. 6.

3.2. Single-core HRSG with one support plate

Case (II) of single-core HRSG with one support plate considers the same operating conditions and optimization formulation as case (I).

The vibration analysis for case (II) is presented in Fig. 5. We first compare the results from the optimizations without the vibration constraints for cases (I) and (II). From the comparison of Figs. 4a and 5a, the tube deflection due to turbulent buffeting is reduced largely for the HRSG with one support plate. Given that the optimized geometries are quite similar (Tables 4 and 6), the reduced deflection is mainly the result of the increased natural frequency due to the halved length of the tube span (Eq. (5)). With the shorter tube span, the allowable critical velocity is increased and the fluidelastic instability criterion is no longer violated.

After adding one support plate to the bundle, only the ratio of f_a/f_{vs} remains almost unchanged, and again acoustic resonance may occur. With the vibration constraints for case (II), the acoustic resonance is avoided by increasing the ratio of f_a/f_{vs} above the upper limit of the lock-in condition, as shown in Fig. 5d. This also results in a slight increase in the ratios y_{rms}/d_o (Fig. 5a) and U_{max}/U_{crit} (Fig. 5c), but they are still inside the acceptable range.

The variables and weight distribution of the optimized HRSGs are listed in Tables 6 and 7, respectively. As with case (I), the solver

with the vibration constraints finds the similar solutions for all the variables except the bundle width. This gives a larger bundle depth but a smaller bundle height. The core volume and heat transfer surface of the tube bundle are almost doubled from the optimization with the vibration constraints. Similarly, the fins and core envelope are the two components having the largest increase in weight. The minimum total weight has increased by 27% compared to the optimization without the vibration constraints, which is far lower than the increase in case (I).

Based on the results of cases (I) and (II), it is found that in general, a shorter tube span either by reducing the tube length or adding one support plate will mitigate the vibration since the shorter span results in a larger stiffness and hence higher natural frequencies. Meanwhile, increased effective mass per unit length by increasing the tube diameter has the same effect. The larger stiffness, higher natural frequencies, and effective mass reduce the vibration and enlarge the allowable critical velocity. Moreover, the fin tip clearance needs to be sufficiently large to limit the gas flow velocity within the acceptable range. In the aspect of the thermal design, denser and larger fins are used to increase the heat transfer area to compensate the lower heat transfer rate due to the smaller gas flow velocity.

The graphic illustration of the HRSGs in cases (I) and (II) is given in Fig. 6. The HRSGs optimized without the vibration constraints have more compact and smaller cores (Fig. 6a and 6c), while the HRSGs optimized with the vibration constraints are opposite (Fig. 6b and 6d). The significant effect of the vibration constraints on the optimized design implies the importance of including vibration analysis to mitigate the risk of flow-induced vibrations when designing a compact and lightweight HRSG.

Table 8
Operating conditions for the three-core HRSG and condenser in case (III).

	Exhaust gas	Steam	Condenser coolant
Flow rate [kg s^{-1}]	130	Optimized	450
Inlet temperature [$^{\circ}\text{C}$]	510	Calculated	10
Inlet pressure [bar]	1.065	40 (HRSG)/ 0.2 (Condenser)	5.0

Table 9
Setting of variables, constraints, and fixed parameters for the optimization in case (III).

Category	Parameter	Value/Range
Variables	Flow rate of steam [kg s^{-1}]	[8,24]
	Bundle width [m]	[4,16]
	No. of support plates [-]	[2,8]
	Fin tip clearance, core 1, 2, 3 [mm]	[2, 45]
Equality constraints	No. of tubes per row, core 1, 2, 3 [-]	[13, 50]
	Power output [MW]	11
Inequality constraint	Equal bundle height, core 1, 2, 3 [m]	Calculated
	Max gas pressure drop [kPa]	3
Fixed	No. of passes, core 1, 2, 3 [-]	6, 4, 4
	No. of rows per pass, core 1, 2, 3 [-]	1, 4, 2
	Tube I.D./O.D., core 1 [mm]	26.7/31.04
	Tube I.D./O.D., core 2 [mm]	33.4/39.14
	Tube I.D./O.D., core 3 [mm]	33.4/39.14
	Fin thickness, core 1, 2, 3 [mm]	1
	Fin height, core 1, 2, 3 [mm]	10
	Fin pitch, core 1, 2, 3 [mm]	6

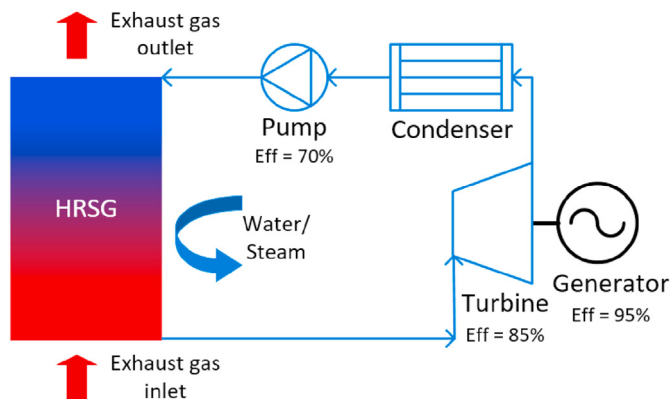


Fig. 7. Layout of a steam Rankine cycle ('Eff' stands for isentropic/mechanical efficiency).

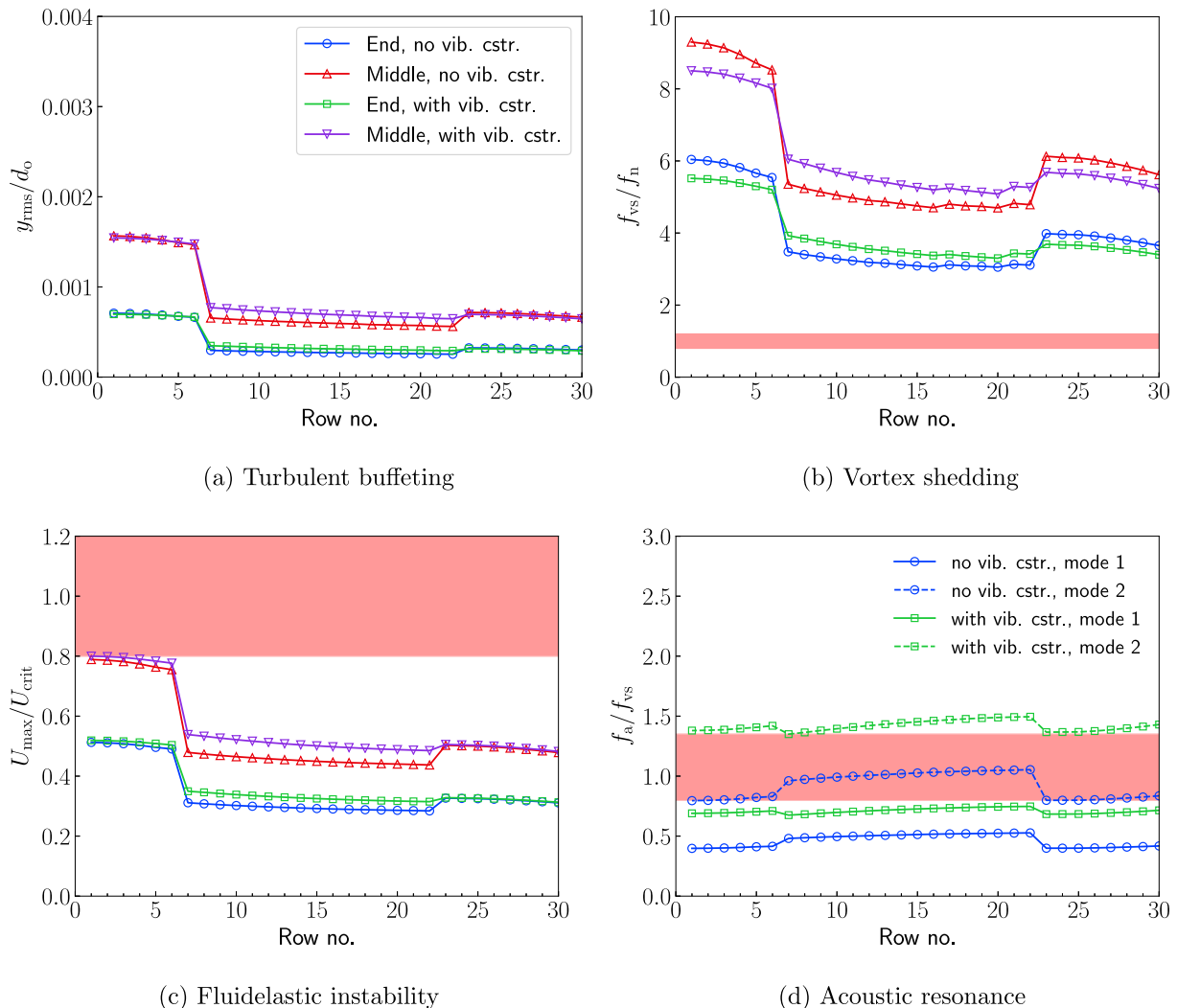


Fig. 8. Comparison of vibrations from the optimizations without and with the vibration constraints for case (III) (End: end span; Middle: middle span). Red region represents the criterion is not satisfied. Row 1–6 are for the superheater, row 7–22 for the evaporator, and row 23–30 for the economizer. (For interpretation of the references to colour in this figure legend, the reader is referred to the Web version of this article.)

3.3. Three-core HRSG with multiple support plates

In case (III), a bottoming cycle in the layout of a simple Rankine cycle is considered as shown in Fig. 7. The cycle consists of a HRSG, a steam turbine connected to a generator, a condenser, and a feed-water pump. The HRSG has three cores: an economizer (core 1), an evaporator (core 2), and a superheater (core 3). The turbine and pump are modeled as an isentropic expansion and compression process with constant isentropic efficiency. Mechanical efficiency is taken into account for losses between the turbine shaft and the generated electrical power. The condenser is modeled based on thermodynamic heat balance, and the pressure drop is neglected.

The operating conditions and the settings for optimization are provided in Tables 8 and 9, respectively. Two identical HRSGs in parallel are used, and the flow rate of exhaust gas in each unit is half of the value in Table 8. In addition to the geometric variables of the HRSG, the operating parameter, flow rate of steam, is also set as a free variable for the optimization. Unlike the fixed value in the previous cases, the number of support plates is a variable. Each of the three cores has individual geometries, while an additional constraint ensures that the cross flow area of the exhaust gas is aligned.

Fig. 8 illustrates the results of the vibration analysis. It can be seen from Fig. 8a that because of the difference in the end fixation of tube spans, the middle spans have larger tube deflection due to turbulent buffeting than the end spans at the same tube row within one optimization. Also, the lower natural frequency of the middle spans results in a smaller allowable critical velocity, and thus a higher possibility of fluidelastic instability as shown in Fig. 8c. In the current case, only the acoustic resonance could be a problem in the optimization without the vibration constraints, given that the ratio f_a/f_{vs} for the second mode falling in the lock-in range (Fig. 8d).

By activating the constraints, the ratio f_a/f_{vs} at mode 1 becomes smaller than the lower limit of the lock-in condition, while the ratio at mode 2 is above the upper limit. This is the combined result of the reduced vortex shedding frequency and increased acoustic resonance frequency. As listed in Table 10, the large decrease in the number of tubes per row gives a smaller bundle height and a larger acoustic resonance frequency. Given that the tube and fin geometry (and the hydraulic diameter) is constant, the increase of fin tip clearance results in a larger tube pitch (a smaller Strouhal number) and a lower gas velocity, which reduces the vortex shedding frequency. The bundle width and the number of support plates are increased to get the required heat transfer area and fulfill the

vibration constraints, respectively.

The weight distributions of the HRSGs optimized with and without the vibration constraints are detailed in Table 11. With the vibration constraints, the weight of the three cores is reduced slightly, while the frame weight is increased and contributes to a larger total weight. This is again due to the overall dimensions of the core. An increase of about 9% in the minimum total weight is

Table 10
Variables of optimized HRSGs for case (III) and calculated geometric parameters.

	Opt. without vib. cstr.	Opt. with vib. cstr.
Steam flow rate [kg s^{-1}]	15.13	13.98
Bundle width [m]	4.45	6.41
No. of support plates [-]	2	3
Fin tip clearance, core 1 [mm]	15.91	23.22
Fin tip clearance, core 2 [mm]	20.81	21.65
Fin tip clearance, core 3 [mm]	12.43	18.62
No. tubes per row, core 1 [-]	35	23
No. tubes per row, core 2 [-]	29	21
No. tubes per row, core 3 [-]	32	22
Bundle height [m]	2.31	1.68
Bundle depth [m]	0.35	0.39
Heat transfer area [m^2]	745.2	717.1
Core volume [m^3]	5.1	5.8

Table 11
Weight distribution of optimized HRSGs for case (III).

Weight [kg]	Opt. without vib. cstr.	Opt. with vib. cstr.
Tube, core 1	1567.5	1449.3
Fin, core 1	1578.4	1487.7
Core 1	3145.9	2937.0
Tube, core 2	6776.8	6529.7
Fin, core 2	4212.4	4357.7
Core 2	10989.2	10887.4
Tube, core 3	3471.6	3206.5
Fin, core 3	2352.8	2263.8
Core 3	5824.4	5470.3
Total of three cores	19959.5	19294.7
Inlet duct	14894.2	16818.6
Core envelope	25548.1	29313.3
Exit duct	5917.3	7007.6
Frame and casing	46359.6	53139.5
Total	66319.1	72434.2

required to satisfy the design criteria. The HRSGs in case (III) are graphically illustrated in Fig. 9. The frame volumes of the two HRSGs are very similar.

4. Conclusion

The design of compact, lightweight, and robust HRSGs is of significance for the implementation of offshore bottoming cycles. A novel methodology for the design optimization of compact HRSG is proposed. The flow-induced vibration analysis, which assists the robustness of the design, is integrated into the formulation of the optimization problem. The sub-models considering four flow-induced vibration mechanisms are implemented for the vibration analysis of the finned tube bundle, and the acceptance criteria are added as inequality constraints. The constrained non-linear optimization problem is solved by NLPQL [43].

The methodology is demonstrated by three representative cases. From the vibration analysis in the first two cases for single-core HRSGs, the results show that fluidelastic instability and acoustic resonance are found to be the most important ones, while turbulent buffeting and vortex shedding is less likely to occur. This result is consistent with the theory by Pettigrew et al. [23]. When activating the vibration constraints, the solver finds appropriate design parameters for tubes and fins geometry so that all design criteria can be met. The total weight of the HRSG without support plates is almost doubled from the optimization with the vibration constraints compared to the one without the vibration constraints, while it increases about 27% for the HRSG with one support plate. In both cases, the solver with the vibration constraints tends to increase the fin tip clearance, so the overall dimensions and volume of the tube bundle are increased. Due to a less compact design and lower gas flow velocities, the heat transfer surface needs to be enlarged to compensate for the lower overall heat transfer rate to retain the required heat duty. This indicates the trade-off between compactness, lightweight, efficient heat transfer, and the possibility of flow-induced vibration problems. It further implies the importance of vibration analysis when designing a highly compact and lightweight HRSG.

The third case for the three-core HRSG in a bottoming cycle demonstrates the methodology with the added complexity of simultaneously optimizing operating parameters together with individual geometric parameters for the three cores. With freely

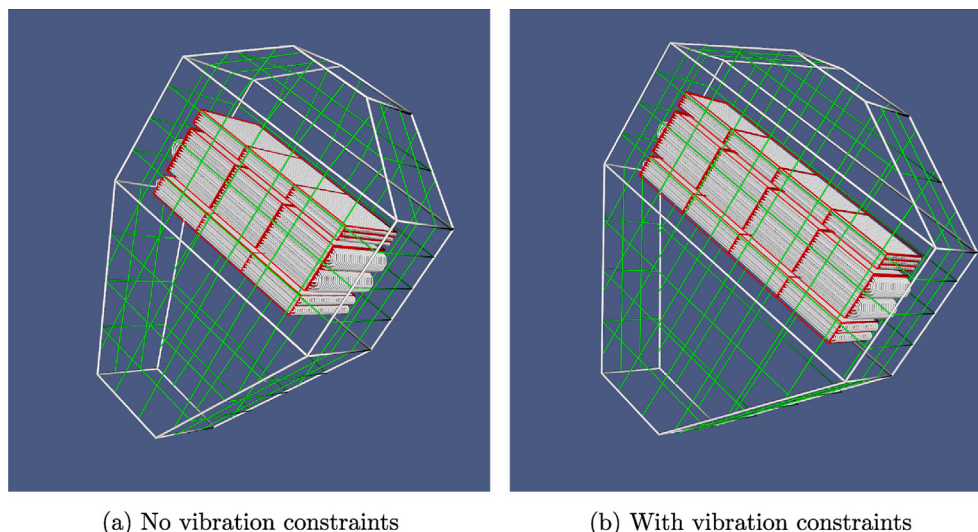


Fig. 9. Visualization of HRSGs optimized for case (III).

selecting the number of support plates, the solver rearranges the tube layout and re-optimizes geometric parameters, so the total weight of the optimized HRSG with the vibration constraints is only increased by 9% compared to the one without the vibration constraints.

The proposed methodology is quite flexible. It can be easily adapted to solve different types of problems by varying the objective functions, such as minimizing the footprint of HRSGs or maximizing the produced power from bottoming cycles. Since the underlying vibrational sub-models for finned tubes are less studied and validated than that for plain tubes, there will be qualitative uncertainties in the presented results. Nevertheless, the methodology will still be applicable when using more accurate sub-models when they are available. Given the capability to optimize operating parameters, it will be useful to embed such methodology into a transient model, which can assist the operation and control strategies for a compact bottoming cycle and thus reduce the risk of damage from flow-induced vibrations.

Credit statement

Han Deng: Methodology, Software, Formal analysis, Writing – original draft, Writing – review & editing, Visualization, Geir Skaugen: Conceptualization, Methodology, Software, Writing – original draft, Software, Writing – review & editing, Erling Næss: Methodology, Writing – original draft, Writing – review & editing, Mingjie Zhang: Writing – original draft, Writing – review & editing, Ole A. Øiseth: Writing – review & editing.

Declaration of competing interest

The authors declare that they have no known competing financial interests or personal relationships that could have appeared to influence the work reported in this paper.

Acknowledgments

The authors acknowledge the partners: ConocoPhillips Scandinavia AS, Equinor Energy AS, NTNU, SINTEF and the Research Council of Norway, strategic Norwegian research program PETRO-MAKS2 (#280713) for their support.

Appendix A. Supplementary data

Supplementary data to this article can be found online at <https://doi.org/10.1016/j.energy.2021.120325>.

References

- [1] Nguyen TV, Voldsund M, Breuhaus P, Elmegaard B. Energy efficiency measures for offshore oil and gas platforms. *Energy* 2016;117:325–40. <https://doi.org/10.1016/j.energy.2016.03.061>.
- [2] Bækken J, Zenker E, Petrofacts. Faktaheftet 2007, tech. Rep. Norwegian Ministry of Petroleum and Energy; 2007. 2007.
- [3] Mazzetti MJ, Nekså P, Walnum HT, Hemmingsen AKT. Energy-efficiency technologies for reduction of offshore CO₂ emissions. *Oil and Gas Facilit*. 2014;3(1):89–96. <https://doi.org/10.2118/169811-PA>.
- [4] Nord LO, Martelli E, Bolland O. Weight and power optimization of steam bottoming cycle for offshore oil and gas installations. *Energy* 2014;76:891–8. <https://doi.org/10.1016/j.energy.2014.08.090>.
- [5] Eriksen VL. *Heat recovery steam generator generator technology*. Elsevier; 2017.
- [6] Franco A, Giannini N. A general method for the optimum design of heat recovery steam generators. *Energy* 2006;31(15):3342–61. <https://doi.org/10.1016/j.energy.2006.03.005>.
- [7] Manassaldi JJ, Mussati SF, Scenna NJ. Optimal synthesis and design of heat recovery steam generation (HRSG) via mathematical programming. *Energy* 2011;36(1):475–85. <https://doi.org/10.1016/j.energy.2010.10.017>.
- [8] Rezaie A, Tsatsaronis G, Hellwig U. Thermal design and optimization of a heat recovery steam generator in a combined-cycle power plant by applying a

- genetic algorithm. *Energy* 2019;168:346–57. <https://doi.org/10.1016/j.energy.2018.11.047>.
- [9] Mehrgoo M, Amidpour M. Constructal design and optimization of a dual pressure heat recovery steam generator. *Energy* 2017;124:87–99. <https://doi.org/10.1016/j.energy.2017.02.046>.
- [10] Mehrgoo M, Amidpour M. Configurations and pressure levels optimization of a heat recovery steam generator using the genetic algorithm method based on the constructal design. *Appl Therm Eng* 2017;122:601–17. <https://doi.org/10.1016/j.applthermaleng.2017.04.144>.
- [11] Skaugen G, Walnum HT, Hagen BA, Clos DP, Mazzetti MJ, Nekså P. Design and optimization of waste heat recovery unit using carbon dioxide as cooling fluid. In: *Proceedings of the ASME 2014 power conference*, vol. 1; 2014. <https://doi.org/10.1115/POWER2014-32165>.
- [12] Païdoussis MP. Real-life experiences with flow-induced vibration. *J Fluid Struct* 2006;22(6–7):741–55. <https://doi.org/10.1016/j.jfluidstructs.2006.04.002>.
- [13] Gawande SH, Keste AA, Navale LG, Nandgaonkar MR, Sonawane VJ, Ubarhande UB. Design optimization of shell and tube heat exchanger by vibration analysis. *Mod Mech Eng* 2011;1(1):6–11. <https://doi.org/10.4236/mme.2011.11002>.
- [14] Fiorentin TA, Mikowski A, Silva OM, Lenzi A. Noise and vibration analysis of a heat exchanger: a case study. *Int J Acoust Vib* 2017;22(2):270–5. <https://doi.org/10.20855/ijav.2017.22.2473>.
- [15] Skaugen G, Kolsaker K, Walnum HT, Wilhelmsen Ø. A flexible and robust modelling framework for multi-stream heat exchangers. *Comput Chem Eng* 2013;49:95–104. <https://doi.org/10.1016/j.compchemeng.2012.10.006>.
- [16] Fong KW, Jefferson TH, Suyehiro T, Walton L. *Guide to the SLATEC. Common Mathematical Library*; 1993.
- [17] Ganapathy V. Industrial boilers and heat recovery steam generators. CRC Press; 2002. <https://doi.org/10.1201/9780203910221>.
- [18] Gnielinski V. New equations for heat and mass transfer in the turbulent flow in pipes and channels. *Int Chem Eng* 1976;16:359–68.
- [19] Bennett DL, Chen JC. Forced convective boiling in vertical tubes for saturated pure components and binary mixtures. *AIChE J* 1980;26(3):454–61. <https://doi.org/10.1002/aic.690260317>.
- [20] Selander W. *Explicit formulas for the computation of friction factors in turbulent pipe flow*, Tech. rep., Chalk River Nuclear Labs. 1978. Chalk River, Ontario.
- [21] Friedel L. Improved friction pressure drop correlations for horizontal and vertical two-phase pipe flow. In: *European two-phase flow group meeting*. Italy: Ispra; 1979.
- [22] Dumont MN, Heyen G. Mathematical modelling and design of an advanced once-through heat recovery steam generator. *Comput Chem Eng* 2004;28(5):651–60. <https://doi.org/10.1016/j.compchemeng.2004.02.034>.
- [23] Pettigrew MJ, Carlucci LN, Taylor CE, Fisher NJ. Flow-induced vibration and related technologies in nuclear components. *Nucl Eng Des* 1991;131(1):81–100. [https://doi.org/10.1016/0029-5493\(91\)90319-D](https://doi.org/10.1016/0029-5493(91)90319-D).
- [24] Taylor CE, Pettigrew MJ. Random excitation forces in heat exchanger tube bundles. *ASME J Pressure Vessel Technol* 2000;122(4):509–14. <https://doi.org/10.1115/1.1286040>.
- [25] Axisa F, Antunes J, Villard B. Random excitation of heat exchanger tubes by cross-flows. *J Fluid Struct* 1990;4(3):321–41. [https://doi.org/10.1016/S0889-9746\(05\)80018-0](https://doi.org/10.1016/S0889-9746(05)80018-0).
- [26] Weaver DS, Ziada S, Sun Z, Feenstra P. The effect of platen fins on the flow-induced vibrations of an in-line tube array. *ASME J Pressure Vessel Technol* 2001;123(4):437–41. <https://doi.org/10.1115/1.1408303>.
- [27] Connors HJ. *Fluidelastic vibration of tube arrays excited by cross flow*. In: *Flow-induced vibration in heat exchangers*. New York: ASME; 1970. p. 42–56.
- [28] Païdoussis MP, Price SJ. The mechanisms underlying flow-induced instabilities of cylinder arrays in crossflow. *J Fluid Mech* 1988;187:45–59. <https://doi.org/10.1017/S0022112088000333>.
- [29] Blevins RD, Bressler MM. Acoustic resonance in heat exchanger tube bundles Part I: physical nature of the phenomenon. *ASME J Pressure Vessel Technol* 1987;109(3):275–81. <https://doi.org/10.1115/1.3264863>.
- [30] Blevins RD, Bressler MM. Acoustic resonance in heat exchanger tube bundles Part II: prediction and suppression of resonance. *ASME J Pressure Vessel Technol* 1987;109(3):282–8. <https://doi.org/10.1115/1.3264864>.
- [31] Païdoussis MP. A review of flow-induced vibrations in reactors and reactor components. *Nucl Eng Des* 1983;74(1):31–60. [https://doi.org/10.1016/0029-5493\(83\)90138-3](https://doi.org/10.1016/0029-5493(83)90138-3).
- [32] Pettigrew MJ, Taylor CE. Vibration analysis of shell-and-tube heat exchangers: an overview Part 1: flow, damping, fluidelastic instability. *J Fluid Struct* 2003;18(5):469–83. <https://doi.org/10.1016/j.jfluidstructs.2003.08.007>.
- [33] Pettigrew MJ, Taylor CE. Vibration analysis of shell-and-tube heat exchangers: an overview Part 2: vibration response, fretting-wear, guidelines. *J Fluid Struct* 2003;18(5):485–500. <https://doi.org/10.1016/j.jfluidstructs.2003.08.008>.
- [34] Blevins RD. *Flow-induced vibration*. New York: Van Nostrand Reinhold; 1977.
- [35] Païdoussis MP, Price SJ, De Langre E. *Fluid-structure interactions: cross-flow-induced instabilities*. Cambridge University Press; 2010. <https://doi.org/10.1017/CBO9780511760792>.
- [36] ESDU. *Flow induced vibration in tube bundles with particular reference to shell and tube heat exchangers*. ESDU Data Item 87019; 1987.
- [37] Bolleter U, Blevins RD. Natural frequencies of finned heat exchanger tubes. *J Sound Vib* 1982;80(3):367–71. [https://doi.org/10.1016/0022-460X\(82\)90277-2](https://doi.org/10.1016/0022-460X(82)90277-2).

- [38] Gelbe H, Ziada S. O2 vibration of tube bundles in heat exchangers. In: VDI heat atlas. Springer Berlin Heidelberg; 2010. https://doi.org/10.1007/978-3-540-77877-6_111.
- [39] Halle H, Chenoweth JM, Wambsgans MW. Flow-induced tube vibration thresholds in heat exchangers from shellside water tests. In: ASME symposium on flow-induced vibration, vol. 3. New Orleans; 1984.
- [40] Weaver DS, Fitzpatrick JA, ElKashlan M. Strouhal numbers for heat exchanger tube arrays in cross flow. ASME J Pressure Vessel Technol 1987;109(2): 219–23. <https://doi.org/10.1115/1.3264899>.
- [41] Singh KP, Soler AI. Mechanical design of heat exchangers and pressure vessel components. ASME J Pressure Vessel Technol 1986;108(3):372–4. <https://doi.org/10.1115/1.3264799>.
- [42] Ziada S, Oengren A, Bhlmann E. On acoustical resonance in tube arrays part II: damping criteria. J Fluid Struct 1989;3(3):315–24. [https://doi.org/10.1016/S0889-9746\(89\)90091-1](https://doi.org/10.1016/S0889-9746(89)90091-1).
- [43] Schittkowski K. NLPQL: a fortran subroutine solving constrained nonlinear programming problems. Ann Oper Res 1986;5:485–500. <https://doi.org/10.1007/BF02022087>.